JOURNAL OF MATERIALS SCIENCE 23 (1988) 2464–2478

# Characterization of $B_2O_3$–$SiO_2$ glasses prepared via sol–gel

M. A. VILLEGAS, J. M. FERNÁNDEZ NAVARRO
*Instituto de Cerámica y Vidrio, CSIC, Arganda del Rey, Madrid, Spain*

$B_2O_3$–$SiO_2$ glasses were prepared by the sol–gel method from boron and silicon alkoxides. The gels were densified by several heat-treatments at temperatures above 800° C. The gel–glass transition was studied with the data obtained from differential thermal analysis, dilatometry and thermal evolution of density. The structural features of the glassy materials prepared were analysed by means of infrared (IR) and near-infrared (NIR) spectroscopy. The IR spectra indicated the existence of mixed Si–O–B bonds, preferential located at the outside of the material particles. The NIR spectra, recorded from gels heat-treated at low temperatures, demonstrated the existence of a great number of $OH^-$ groups varying in nature, as well as their evolution and their positional changes on the silica particle surface as a function of the heat-treatment.

## 1. Introduction

The sol–gel method for making glasses at low temperatures has undergone successful further development in the last few years. The products obtained, such as fibres, coatings and bulk glasses, possess certain features and properties which make them suitable for highly specific applications (optical fibres, reactive powders, foams, catalysts, hollow spheres, nuclear waste fixation ceramic–metals, composites, glass–ceramic polymer composites, reflective and anti-reflective coatings, monoliths without melting, etc. [1]).

Gels and glasses of the system $B_2O_3$–$SiO_2$ have been widely researched by several authors. Basically two methods have been developed for the preparation of these materials:

(a) from colloidal $SiO_2$ solutions with the addition of boric acid or a boron salt [2–5], and
(b) by means of hydrolysis and polycondensation of silicon and boron alkoxides [6–11].

From the point of view of gel drying and heat-treatment to achieve the gel–glass conversion, the work carried out to date can be classified in three groups:

(i) xerogel preparation and glass transformation by means of heat-treatments in air [3, 6, 9, 11];
(ii) xerogel preparation yielding glasses by the pressing of powders obtained from heat-treatments [4, 5, 10]; and
(iii) preparation of aerogels through drying in an autoclave under hypercritical conditions [8].

This paper reports on the preparation of xerogels of the system $B_2O_3$–$SiO_2$ from alkoxides which were heat-treated until reaching maximum densification without hot-pressing. The main purpose in this research was to characterize these materials and to study their thermal and structural evolution.

## 2. Experimental procedure

### 2.1. Sol preparation

Four compositions of the $B_2O_3$–$SiO_2$ system were prepared (Table I) using tetraethylorthosilicate (TEOS) as $SiO_2$ source and trimethylborate (TMB) as $B_2O_3$ source.

TEOS was diluted with ethanol (4 ml ethanol per 20 g end-product) and then the mixture was hydrolysed with 0.15 N HCl. The molar ratio to water of the sum of alkoxide molecules (TEOS + TMB) : $H_2O$ was adjusted to 1 : 1.5 in order to avoid $H_3BO_3$ precipitation. After a few minutes of vigorous stirring a clear and homogeneous solution was obtained, to which TMB was added. Stirring was maintained for another half-hour. Then the sols were covered with a plastic sheet, sealed and placed in a forced-air stove at 60° C.

For near-infrared (NIR) spectra recordings (4200 to 8000 $cm^{-1}$) samples in the form of thin planoparallel gel sheets were prepared in glass petri dishes, with thickness varying between 1 and 2 mm.

### 2.2. Gelling, drying and heat-treatment

Sols gelled at 60° C in the course of 24 to 48 h, depending on their composition. They were then dried at that temperature for 4 to 6 days. The sol samples for NIR recordings also gelled at 60° C, yet at much shorter gelling times due to their small volume in

TABLE I Sample compositions

| Sample No. | Composition (mol %) | |
|---|---|---|
| | $B_2O_3$ | $SiO_2$ |
| 3.1 | 40 | 60 |
| 3.2 | 30 | 70 |
| 3.3 | 20 | 80 |
| 3.4 | 10 | 90 |



0022–2461/88 $03.00 + .12 

the petri dishes. Once the gels had dried they were heat-treated at different temperatures to achieve maximum densification.

Heat-treatments at 130 and 200° C were performed in a forced-air stove which was equipped with a programmer. The following schedules were achieved:

(i) Heating rate 0.1° C $min^{-1}$ up to 130° C and stabilization 10 h at 130° C, and
(ii) heating rate 0.2° C $min^{-1}$ up to 200° C and stabilization 10 h at 200° C.

Heat-treatments up to 300, 550 and 850° C were applied in a muffle furnace, provided with a programmer:

(i) Heating rate 1.25° C $min^{-1}$ up to 300° C and stabilization 10 h at 300° C;
(ii) heating rate 1.25° C $min^{-1}$ up to 550° C and stabilization 6 h at 550° C;
(iii) heating rate 1.25° C $min^{-1}$ up to 200° C, stabilization 2 h at 200° C, heating rate 1.25° C $min^{-1}$ up to 850° C and stabilization 12 h at 850° C.

The samples subjected to heat-treatments up to 300, 550 and 850° C were pre-treated at 130° C following the schedule indicated above.

### 2.3. Gel characterization

Differential thermal analysis (DTA) and thermogravimetric analysis (TGA) diagrams were recorded on a Mettler instrument using a platinum crucible and a heating rate of 10° C $min^{-1}$. $Al_2O_3$ was used as reference substance.

The X-ray diffraction data were recorded in a Philips apparatus model PW-1140/1370/1540.

Sample densities were measured by means of a direct method determining mass and volume. Sample volume determination was performed in powder specimens using toluene as reference liquid in a pycnometer. The measurements were repeated three or four times for each gel treatment temperature.

The infrared (IR) spectra were obtained from powdered gels using the technique of anhydrous KBr pellets. The spectra was recorded with a Perkin-Elmer spectrophotometer Model 580B. The NIR spectra were recorded on a Perkin-Elmer Model Lambda 9, from samples in the form of thin sheets.

Gel contraction during densification was followed on an ISA (France), Adamel Lhomargy dilatometer Model DI 24 with heating rates of 1° C $min^{-1}$ and $Al_2O_3$ as support substance. The samples were strictly planoparallel, thickness varying from 2 to 5 mm. These samples were prepared from gel pieces polished with silicon carbide paper.

## 3. Results and discussion

### 3.1. DTA–TGA diagrams and X-ray diffraction

The DTA–TGA diagrams of the gels in Fig. 1 show an endothermic peak between 115 and 141° C, due to the loss of adsorbed water and methyl and ethyl alcohols derived from TMB and TEOS hydrolysis, respectively. The appearance of similar endothermic peaks has been observed in previous research for alkaline silicate gels [12, 13] and for $Na_2O$–$B_2O_3$–$SiO_2$ gels [14]. Fig. 1 shows these peaks to become progressively higher as a function of increasing $B_2O_3$ content in the gels. This fact is easy to explain, taking into account that on increasing the molar amount of $B_2O_3$ the silicon alkoxides mols will diminish proportionately. As a consequence, the amount of water present (incorporated as 0.15 N HCl) will also increase in order to maintain the molar ratio of water to the sum of alkoxides at 1.5. In Fig. 2 weight loss, as a percentage from the TG curves, has been plotted against temperature. The weight loss of the first endothermic peak in the DTA diagrams is completed between 250 and 300° C.

All the diagrams in Fig. 1 show two exothermic peaks near 300° C. The first of these peaks decreases with regard to the second as a function of the $SiO_2$ content in the samples. By the same token, the second peak increases proportionately. In the TG curves weight losses are shown to set in with the first exothermic peak, and to end within the range of the second. Taking into account sol preparation, 1.5 moles of water per mole of (TEOS + TMB), it can be expected that neither the TEOS nor the TMB have been totally hydrolysed, since a TEOS molecule requires four water molecules for full hydrolysis and a TMB molecule needs three. Hence, after gelling there remain organic groups ($EtO^-$ and $MeO^-$). Thus units $Si(OH)_x(OC_2H_5)_{4-x}$ and $B(OH)_y(OCH_3)_{3-y}$ can subsist up to 300 and 360° C, where combustion of organic groups sets in. Consequently, the first exothermic peak, which increases with the $B_2O_3$ content, is attributable to the combustion of residual $MeO^-$ groups which were not hydrolysed prior to gelling. These groups increase with the TMB concentration in the sols. The second exothermic peak, which increases with increasing $SiO_2$ content, is due to the combustion of the $EtO^-$ groups which were not previously hydrolysed. These groups increase with the amount of TEOS used for sample preparation.

In Fig. 2 it can be observed that in the temperature range between 250 to 300° C and 900° C, Sample 3.1 shows a relatively small weight loss. For Samples 3.2 and 3.3 the weight loss is practically of the same order of magnitude. For Sample 3.4, however, it is substantially higher. This result was to be expected, since on increasing the silica content the number of $EtO^-$ groups to be eliminated also grows. In addition, $EtO^-$ groups represent a greater mass than $MeO^-$ groups.

In the DTG curves two peaks can be observed for each sample. The first of these diminishes proportionate to $SiO_2$ increase in the gels, and the second increases with $SiO_2$. This fact allows the inference that the second peak increases at the cost of the first. In other words, the gels contain a number of alcohols and organic groups to be eliminated. Should it be the case that during a first stage a great part of the alcohol has not been released (first peak), during a second stage many OR groups will have to be eliminated (second peak) and vice versa. This means that all residual OR groups which remain unhydrolysed prior to gelling, due to the small amount of water used, will be eliminated at a later stage in the combustion process.

The X-ray diffraction data show that in the

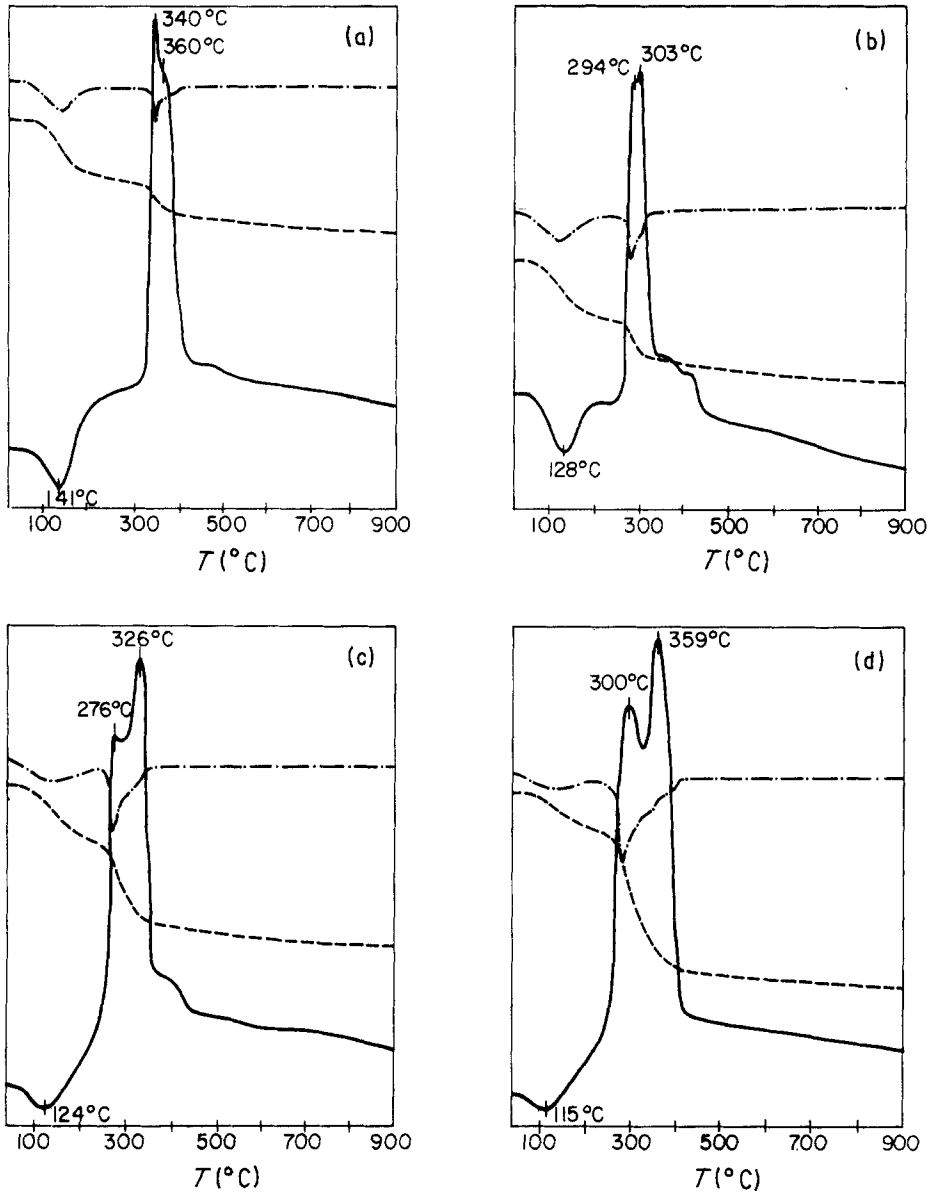


*Figure 1* DTA-TGA diagrams of the samples: (a) 3.1, (b) 3.2, (c) 3.3, (d) 3.4: (——) DTA, (– – –) thermogravimetry (TG), (—·—) derivative TG.

temperature range between 130 and 850° C no crystallization whatsoever is produced. In contrast to the alkaline silicate gel glasses [13] and $Na_2O$–$B_2O_3$–$SiO_2$ gel glasses [14] which do present crystallization once a certain temperature range has been achieved, the gels of the $B_2O_3$–$SiO_2$ system remain amorphous, as has been also observed by other authors [4]. Phalippou *et al.* [3] observed silica crystallization (cristobalite) in $B_2O_3$–$SiO_2$ gel glasses with 5 to 10 mol%. These materials were prepared from colloidal silica solutions and inorganic boron compounds. The same authors, however, did not observe any crystallization for pure silica gels prepared from alkoxide hydrolysis and polycondensation. The reason why gels prepared from solutions crystallize is to be sought in the presence of impurities, specifically a certain alkali concentration, which affects the thermal evolution of the gel surface [3]. This fact was already confirmed in previous studies [13, 14], which referred to $Na_2O$-containing gel glasses. In the gels prepared and studied in this work, no crystallization appeared. This is not so much due to densification at lower temperatures than required for crystallization to occur (850° C) [3], but is mainly attributable to the fact that the preparation method was the hydrolysis and condensation of very pure organometallic compounds. Organometallics in themselves attenuate and delay [3, 4] the possibilities for crystallization to occur. According to Jabra *et al.* [4] the $B_2O_3$ acts as an inhibitor of the crystallization trend in silica gels.

## 3.2. IR and NIR spectra

The IR spectra of the gels (300 to 4000 $cm^{-1}$) are shown in Figs 3 to 6. The main absorption band assignment, based on previous studies [4, 6, 7, 10, 11] is shown in Table II.

The O–Si–O deformation vibration band [4, 10, 11] is situated at 450 to 460 $cm^{-1}$ and is seen to become more intense and more clearly outlined with increasing heat-treatment temperature. This effect is even more noticeable when the silica content is increased in gels heat-treated at 200 and 300° C. At the same time the band is displaced towards higher wave-numbers. At higher temperatures (550 to 850° C) the bands

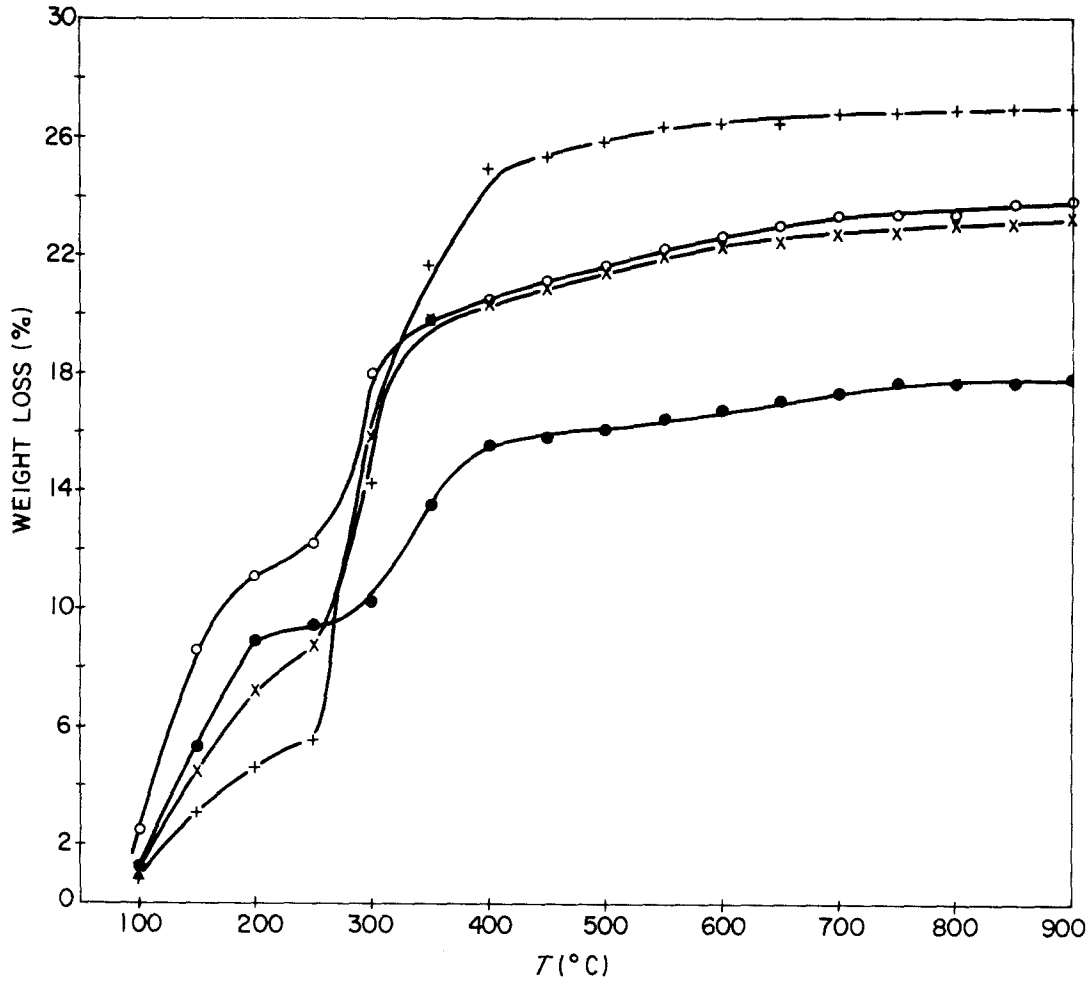


*Figure 2* Weight loss (%) of the samples as a function of heat-treatment temperature: (●) 3.1, (○) 3.2, (x) 3.3, (+) 3.4.

do not vary their intensity as a function of sample composition. The band corresponding to the ring structure vibrations of the $SiO_4$ groups (850° C) [4, 7, 10, 11] does not show any remarkable change due to gel composition. It only becomes more intense as a consequence of the formation of a larger number of Si–O–Si links in the network with heat-treatment. Other authors [7, 15] have assigned this band to the Si–O–Si bending vibration and to the symmetric Si–O stretching vibration [16]. Around 1090 to 1100 $cm^{-1}$ there appears the band corresponding to the asymmetric stretching vibration (transverse optical mode) [7] of the Si–O bond [4, 6, 10, 11]. This band moves towards higher wave-numbers if the gel treatment temperature is increased, although it hardly changes in intensity with regard to gel composition. The shoulder, however, which is situated near 1200 $cm^{-1}$ and is assigned to the asymmetric Si–O stretching vibration (longitudinal optical mode) [7] becomes more diffuse with increasing heat-treatment temperature and remains practically invariable with changes in sample composition.

The position and evolution of these four absorption bands assigned to the silica network suggest that, on the whole, they experience only minor alterations due to variations in sample composition. They seem, however, to be sensitive to the thermal evolution of the gels, in the sense that they become more intense or they move towards higher wave-numbers, which is indicative of a reinforcement of the Si–O bonds. As a matter of fact, the densification through heat-treatment and independent of $B_2O_3$ content translates

TABLE II IR wave-numbers and vibration band assignments

| $\bar{\nu}$ ($cm^{-1}$) | Assignment | References |
|---|---|---|
| 1630 | H–O–H deformation | 10 |
| 1400 | B–O stretching | 6, 7 |
| 1200 | Asymmetric Si–O stretching (longitudinal optical mode) | 7 |
| 1090 | Asymmetric Si–O stretching (transverse optical mode) | 4, 6, 7, 10, 11 |
| 945 | Si–OH stretching | 6, 7, 11 |
| 915 | Si–O–B stretching | 4, 6, 7 |
| 800 | [$SiO_4$] tetrahedron rings | 4, 7, 10, 11 |
| 670 | Si–O–B deformation | 4, 6, 7, 11 |
| 460 | O–Si–O deformation | 4, 10, 11 |

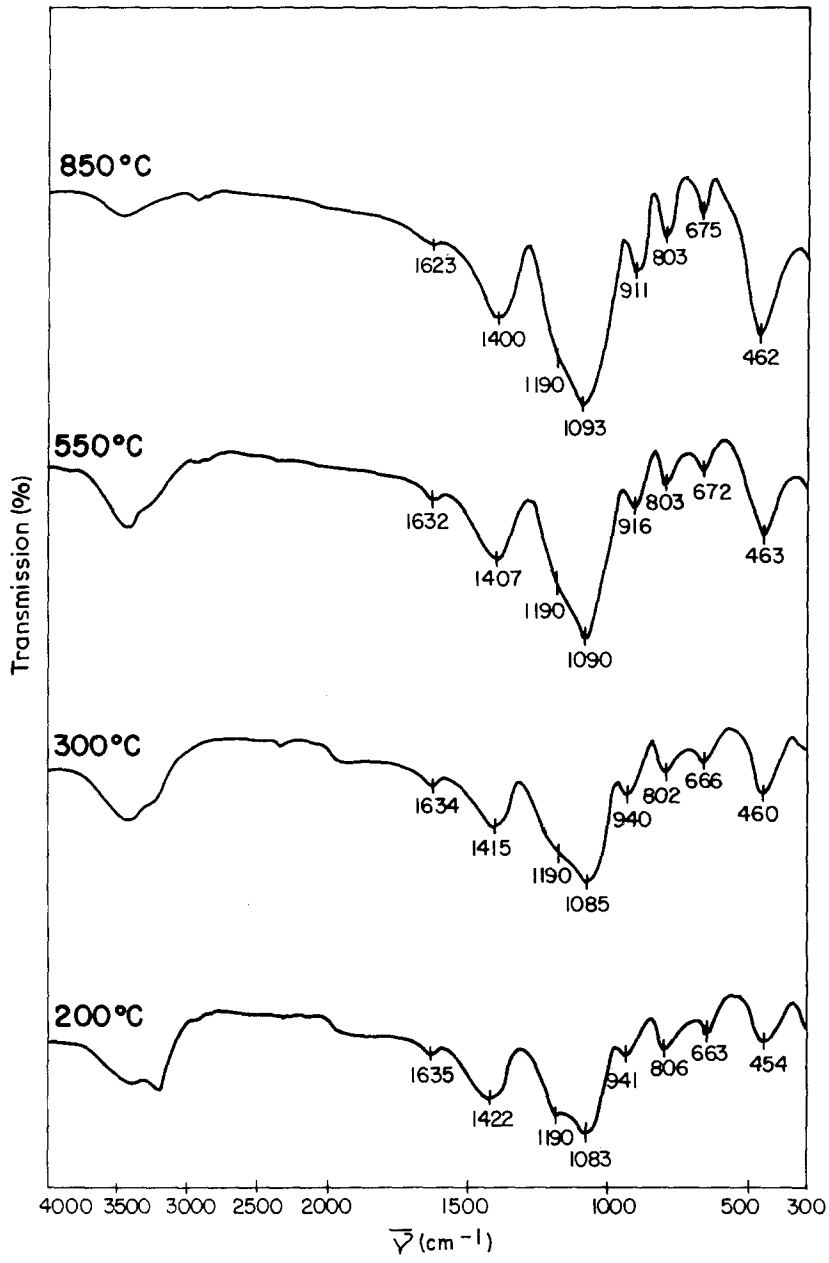


*Figure 3* IR spectra of Sample 3.1 as a function of heat-treatment temperature.

into an increase of Si–O links (Si–O–Si or Si–O–B bonds) formed from silanol groups. On the other hand, greater densification can also account for the formation of stronger links in a more compact network and, consequently, the displacement of vibration frequencies towards higher wave-numbers. The fact that bands belonging to the silica network are obviously not influenced by the presence of greater or lesser $B_2O_3$ amounts is due to the particular nature of the gel. The gels consist of silica particles of a certain size and degree of polymerization, on whose surface the boron atoms are situated [11], as will be discussed below. Hence the silicon and oxygen atom clusters lodged in the innermost part of the particles remain virtually unaltered by compositional $B_2O_3$ variations.

The band assigned to the Si–OH stretching vibration, around 940 to 950 cm$^{-1}$ [6, 7, 11], is only present in the spectra of samples treated at 200 and 300° C and does not vary in intensity as a function of compositional changes. This is logical taking into account the condensation process taking place near 550° C. During this process the chemically bonded water is released giving rise to Si–O–Si and Si–O–B bonds at the expense of the Si–OH and Si–OR groups. This is confirmed by the fact that the absorption band near 915 cm$^{-1}$ and attributed to the Si–O–B stretching vibration [4, 6, 7] begins to appear at 550° C at the expense of the Si–OH band [7]. On the other hand, the Si–O–B vibration band is observed to grow with increasing heat-treatment temperature in the gels containing a large $B_2O_3$ percentage (Samples 3.1 and 3.2). By the same token, this band diminishes markedly on increasing the silica content. The band near 670 cm$^{-1}$ assigned to the Si–O–B deformation vibration [4, 6, 7, 11] also increases with treatment temperature and moves towards greater wave-numbers, indicating a reinforcement of the bonds in the gels with a larger $B_2O_3$ amount. This band diminishes its intensity rapidly on increasing the silica percentage, especially in samples treated at 550 and 850° C. The results obtained indicate that the Si–O–B links are fundamentally terminal in the gels treated at low

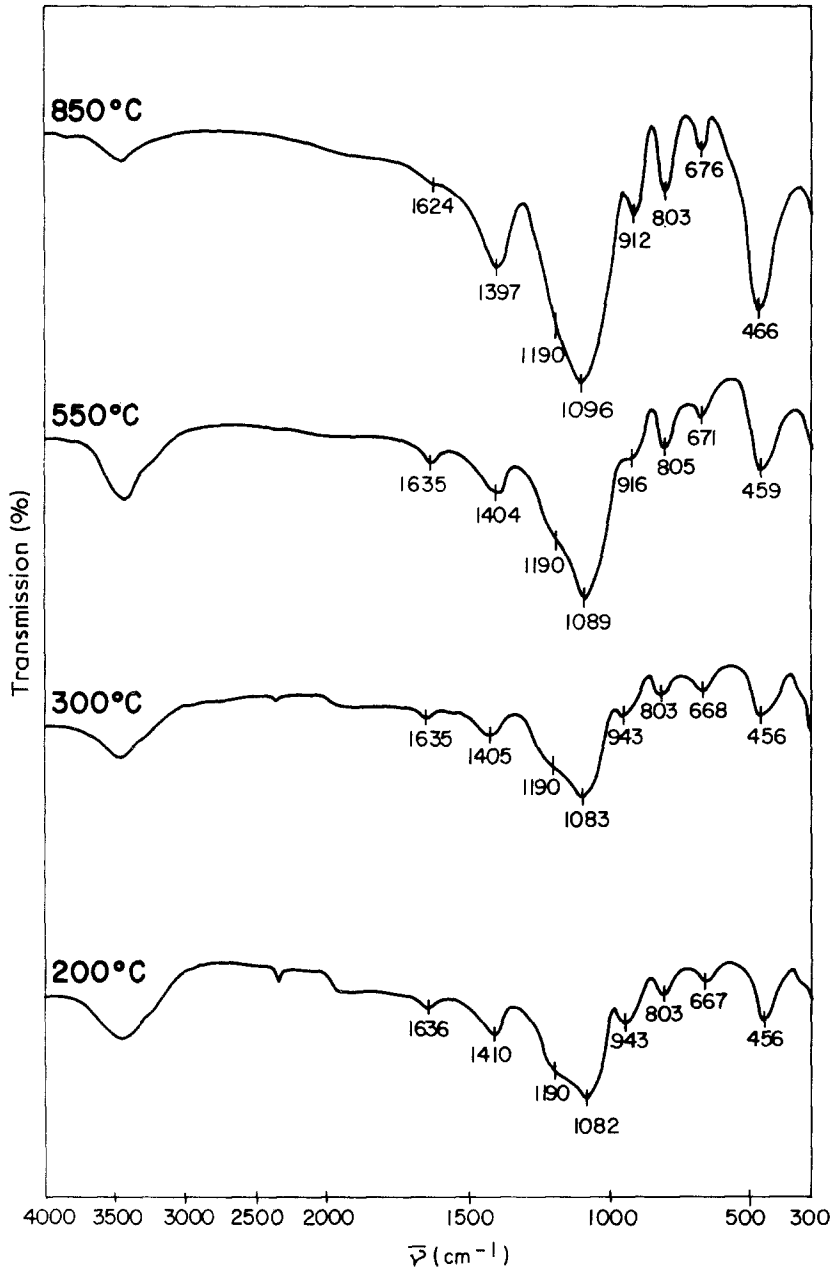


*Figure 4* IR spectra of sample 3.2 as a function of heat-treatment temperature.

temperatures. The structures would be basically as follows:

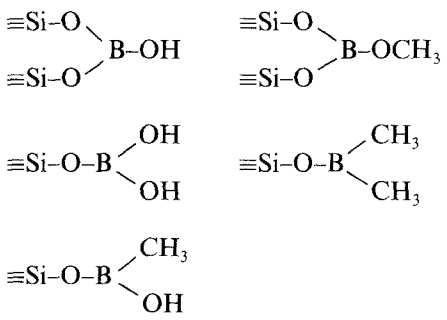

At high temperature the OH and/or $CH_3$ groups are eliminated giving rise to condensations of the type

$$\equiv Si-O-B-O-Si\equiv$$

This situation can supply an explanation for the band displacement towards higher wave-numbers at 500 and 850° C.

The band assigned to the B–O stretching vibration at 1400 cm$^{-1}$ [6, 7] appears with clear outlines if the heat-treatment temperature is increased. Enhancement of band intensity with temperature is explained through B–OH groups incorporation [7] into the borosilicate phase, during which Si–O–B bonds are progressively formed. As has been pointed out in the literature [7], this band moves towards lower wave-numbers and grows in intensity on treating the samples with a larger $B_2O_3$ amount thermically in air. The initial appearance of this band at higher wave-numbers indicates that, at low temperatures, the non-bridge B–O bonds are predominant.

Finally, around 1630 cm$^{-1}$ [10] the deformation vibration of physically adsorbed molecular water appears. This band diminishes and is displaced towards lower wave-numbers on increasing heat-treatment temperature. In the samples treated at 850° C it is very small and is probably due to adsorbed water from the atmosphere during sample handling for the spectrum recording.

The fact that there does not appear any absorption band around 720 cm$^{-1}$ (B–O–B deformation vibration) [4, 6] and that the intensity of the bands corresponding

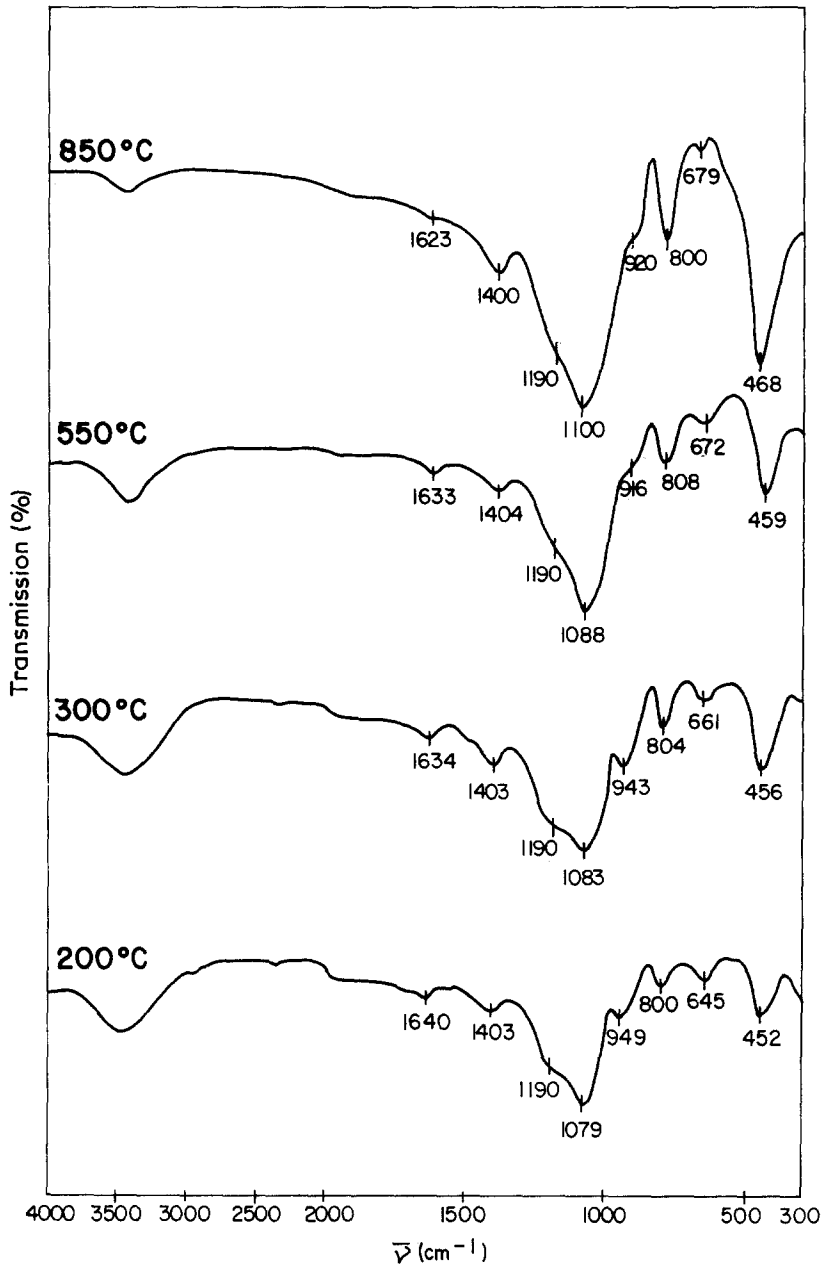


*Figure 5* IR spectra of sample 3.3 as a function of heat-treatment temperature.

to the stretching vibration (915 cm$^{-1}$) and deformation vibration (670 cm$^{-1}$) of the Si–O–B links grow with $B_2O_3$ content in the samples, suggests that all the $B_2O_3$ incorporates into the network to form Si–O–B links, but not B–O–B bonds. This has also been observed by other authors [6] in gels of the $B_2O_3$–$SiO_2$ system.

Near-infrared spectroscopy constitutes a good technique to study the thermal evolution of water in conventional hydrated glasses [17–21], as well as in gel-derived glasses [22–25]. Moreover, in these latter it is possible to study the elimination of residual organic groups after hydrolysis of the final oxide precursor alkoxides. Figs 7 and 8 show the NIR spectra (4200 to 8000 cm$^{-1}$) of the gels treated at low temperatures (130, 200 and 300° C). Band assignment based on previous studies [17–24] is compiled in Table III.

The effect of $B_2O_3$ concentration in the gels is shown in Fig. 7. At 130 and 300° C, evolution as a function of sample composition is very similar to that represented in Fig. 7. The band situated around 7300 cm$^{-1}$ and attributed to the first overtone of the O–H stretching vibration of the free isolated silanol groups [17, 19–22] (Fig. 9a) does not show any significant alterations in the four samples. The same situation is observed for the first overtone (7194 cm$^{-1}$) of the O–H stretching vibration of the water molecules hydrogen-bonded to the neighbouring silanol groups [22, 23] (Fig. 9b). For Sample 3.4 there appears a band at 7092 cm$^{-1}$ assigned [23] to the first overtone of the O–H vibration of the neighbouring silanols hydrogen-bonded to water molecules (Fig. 9b). The other three samples, however, present a shoulder at 7092 cm$^{-1}$ which becomes more intense when increasing the silica content.

At 5917, 5780 and 5682 cm$^{-1}$ the triplet of the first overtone of the fundamental C–H vibration appears [23], which is present in the gels due to incomplete hydrolysis of the alkoxides. The triplet is present in the four gels with similar features, as at 200° C the organic residual groups has not yet been totally eliminated. The combined stretching–bending combination band of the water hydrogen-bonded to neighbouring silanol groups [19–22] appears near 5263 cm$^{-1}$ (Fig. 9b). This

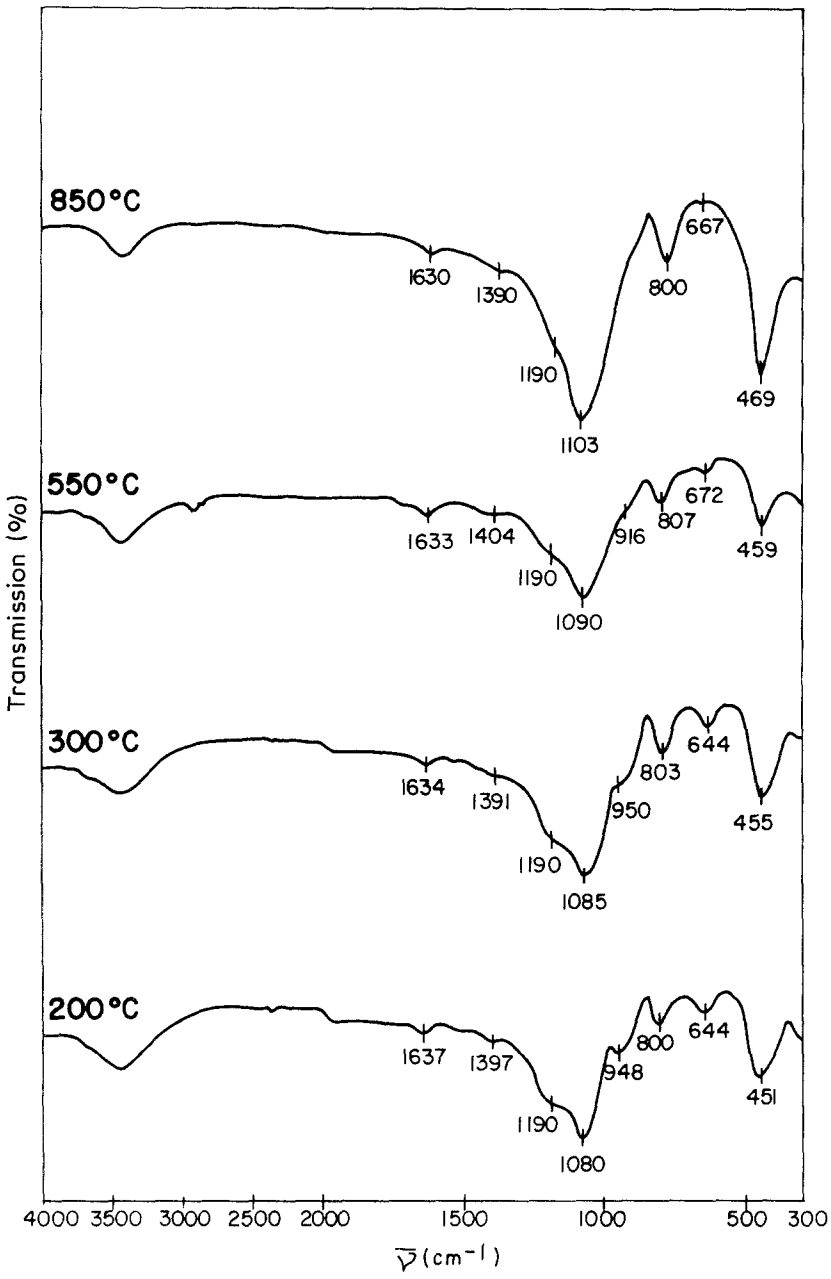


*Figure 6* IR spectra of sample 3.4 as a function of heat-treatment temperature.

TABLE III NIR-wave-numbers and vibration band assignments

| $\bar{\nu}$ (cm$^{-1}$) | Assignment | References |
|---|---|---|
| 7300 | First overtone of the O–H stretching vibration of the free isolated silanol | 17, 19–22 |
| 7194 | First overtone of the O–H stretching vibration of the water hydrogen-bonded to neighbouring silanols | 22, 23 |
| 7092 | First overtone of the O–H vibration of the neighbouring silanols hydrogen-bonded to water | 23 |
| 5917<br>5780<br>5682 | First overtone of the fundamental C–H vibration | 23 |
| 5263 | Stretching–bending combination of the water O–H hydrogen-bonded to neighbouring silanols | 19–22 |
| 5050 | Stretching–deformation combination of water hydrogen-bonded to neighbouring silanols forming clusters | 22 |
| 4878 | O–H stretching–deformation combination of ethanol | 23, 24 |
| 4545<br>4425 | O–H stretching–bending combination of free silanols or hydrogen-bonded neighbouring silanols | 17–22 |
| 4348 | Stretching–deformation combination of the neighbouring silanols hydrogen-bonded to water forming clusters | 22 |
| 4274 | C–H stretching–deformation combination | 23 |

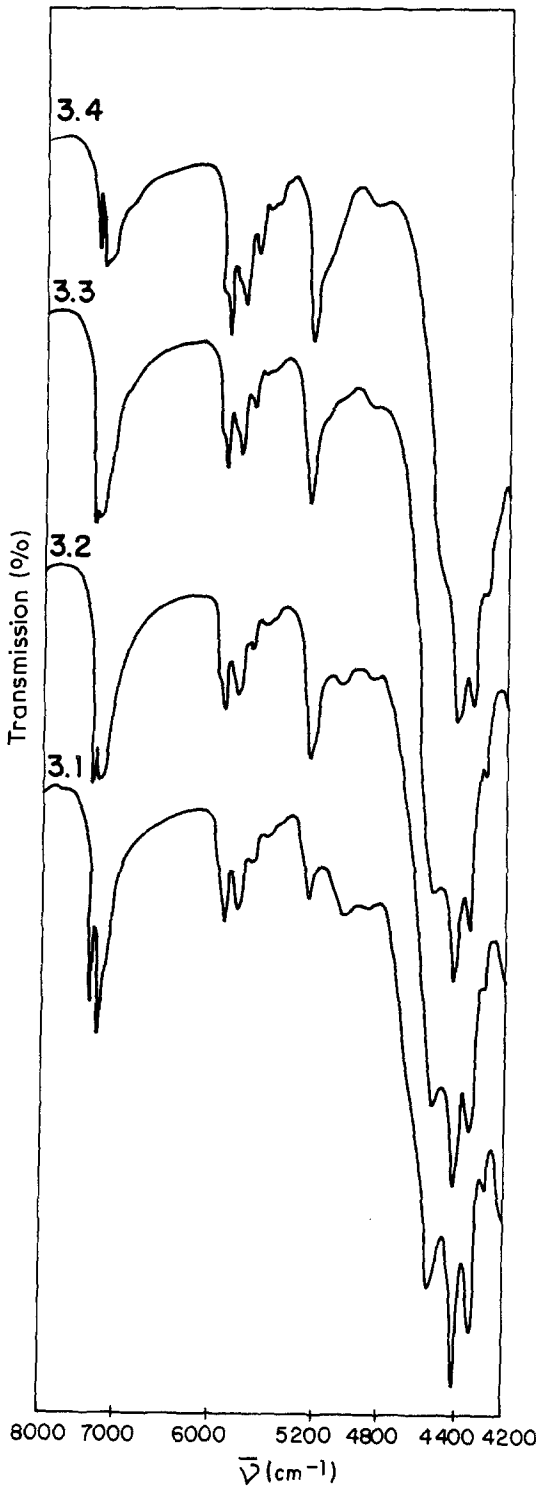


*Figure 7* NIR spectra of the samples at 200° C.

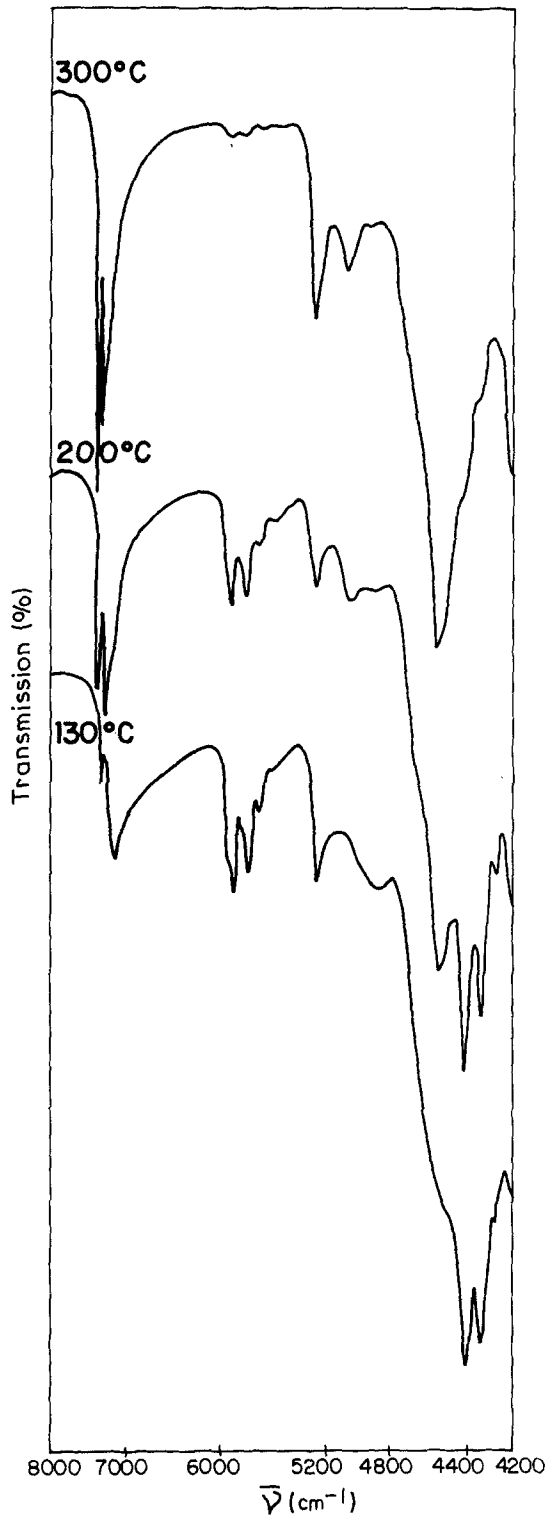


*Figure 8* NIR spectra of Sample 3.1 as a function of heat-treatment temperature.

band intensifies on increasing the silica percentage in the samples. The stretching–deformation combination band at 5050 cm$^{-1}$, assigned to the O–H of the water molecules hydrogen-bonded to neighbouring silanol groups forming clusters [22] (Fig. 9d), does not increase, but even diminishes with greater silica content. The relative behaviour of the bands at 5263 and 5050 cm$^{-1}$ suggests that the first grows at the expense of the second with increasing silica content. This situation is understandable, considering that on increasing the silica content there are more silanol groups available to form structures of the type shown in Fig. 9b, whose water molecules would be taken from the more external ones in the clusters shown in Fig. 9d.

The O–H stretching–deformation combination of ethanol has been assigned [23, 24] to the band situated near 4878 cm$^{-1}$. This band is relatively small in all gels, pointing towards a limited amount of physically adsorbed ethanol. At 300° C it is practically eliminated, as will be shown below.

At 4545 and 4425 cm$^{-1}$ there appear other stretching–bending combination bands of the O–H in the free silanols, as observed in fused silica glass [17] and silicate glasses [18–21]. These bands were also assigned [22] to the same vibration mode of silanol groups hydrogen-bonded to water molecules (Fig. 9b). Both

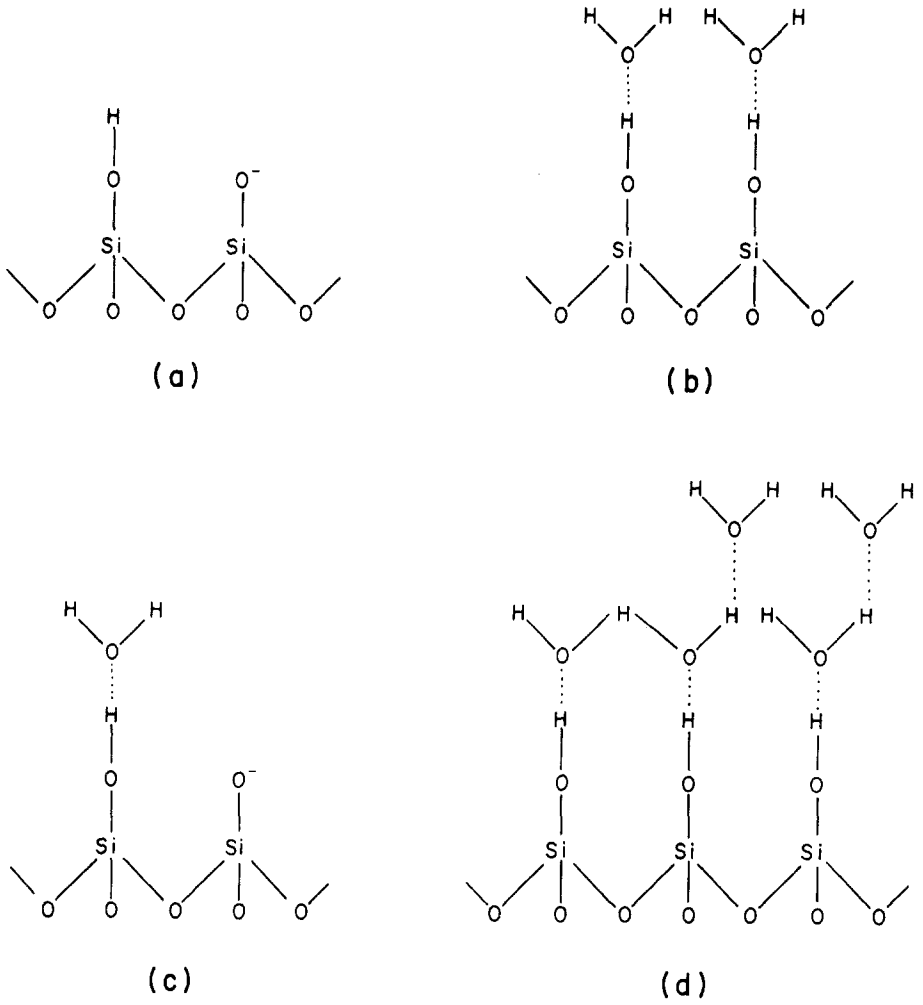


*Figure 9* Schematic representation of the molecular structures present in a pure silica gel according to Wood *et al.* [22].

bands are present in the spectra of all samples but are more sharply defined in the gels with larger amounts of $B_2O_3$. The stretching–deformation combination referring to the neighbouring silanols hydrogen-bonded to water molecules forming clusters [22] (Fig. 9d) have been assigned to the band situated at 4348 $cm^{-1}$. This band is intense in all the samples. At 4274 $cm^{-1}$ there appears a band that has been assigned [23] to the C–H stretching–deformation combination. Although it is not very strong, it appears in all the samples, since at 200° C there still remain organic groups from the alkoxides.

The thermal evolution of the bands assigned for Sample 3.1 in Table III is shown in Fig. 8. The other three gels show a practically identical thermal behaviour.

The most important effects observed as a consequence of temperature rise are the following:

(a) all the bands due to organic groups (5917, 5780, 5682, 4878 and 4274 $cm^{-1}$) diminish or practically disappear at 300° C;

(b) the bands attributable to the O–H of the free silanols (7300 $cm^{-1}$) and to the O–H of neighbouring silanols hydrogen-bonded to water molecules (7092 and 4545 $cm^{-1}$) intensify with temperature;

(c) the bands corresponding to the O–H of water hydrogen-bonded to neighbouring silanols (7194 and 5263 $cm^{-1}$) remain with similar intensities or increase;

(d) the band due to the O–H of free silanols or hydrogen-bonded to water molecules (4425 $cm^{-1}$) diminishes as a function of rising temperature; and

(e) the O–H band of water hydrogen-bonded to neighbouring silanols forming clusters (5050 $cm^{-1}$) increases, while the respective O–H band of the silanols of the same structure (4348 $cm^{-1}$) decreases with temperature.

Assuming that the initial surface of a gel particle is similar to the situation represented in Fig. 9d, the band reduction as a function of temperature rise shown by the O–H band of those silanols does find a sensible explanation. The water molecules are progressively eliminated, giving rise to any of the other structures in Fig. 9. Later on, the same evolution takes place for the O–H of the silanols in Fig. 9c, from which the water is lost, thus originating new free isolated silanol groups (Fig. 9a). The O–H band increase with temperature of the free isolated silanols is due to the fact that this is one of the least hydrated structures and it can therefore be preserved up to very high temperatures [22, 23]. Dehydration of the structure shown in Fig. 9d can furthermore explain the generation of neighbouring silanol groups hydrogen-bonded to water molecules (Fig. 9b). Thus the increase in intensity of the O–H bands of the silanols and the O–H of the water molecules of such structures can be explained. Contrary to expectations, the O–H band of the water molecules in Fig. 9d increases with temperature. The vibration assigned to these molecules is similar to that of free water, following the interpretation proposed by other authors [22]. It is possible that the band at 5050 $cm^{-1}$, apart from being due to the water molecules of the structure in Fig. 9d, also

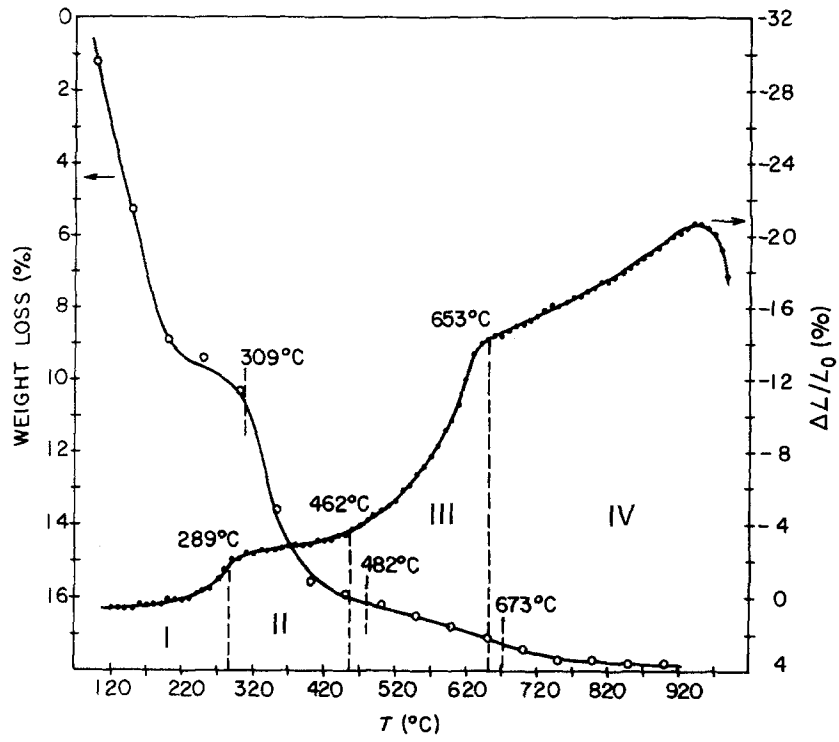


*Figure 10* Linear contraction and weight loss of sample 3.1.

refers to water molecules generated in the incipient silanol group condensation process. In this case the intensity increase of the band could be explained. In this context, the fact acquires specific significance that the NIR spectra were recorded in a narrow temperature range (130 to 300° C) of heat-treatments, where abundant O–H bonds of different types are still present.

### 3.3. Gel densification

Figs 10 to 13 show the linear contraction percentages ($\Delta L/L_0$) of the gels as a function of temperature. They also include the respective weight loss percentages. Although the weight loss data were calculated from the TGA curves recorded at a heating rate of $10°\,C\,min^{-1}$ and the dilatograms were recorded at a rate of $1°\,C\,min^{-1}$, these curves allow for qualitative comparison. The retarded effects observed in the weight-loss curves were due to the higher heating rate.

Assuming that densification is an activated process, the sample length variation at a given temperature $T$ (K) can be expressed by the following equation:

$$\Delta L = L_0 e^{-E_a/RT} \quad (1)$$

where $L_0$ stands for initial length, $E_a$ is the process activation energy and $R$ is the gas constant. Employing Napierian logarithms we obtain

$$\ln\left(\frac{\Delta L}{L_0}\right) = \left(\frac{-E_a}{1000R}\right)\left(\frac{1000}{T}\right) \quad (2)$$

where $-E_a/1000R$ is the slope of the straight line.

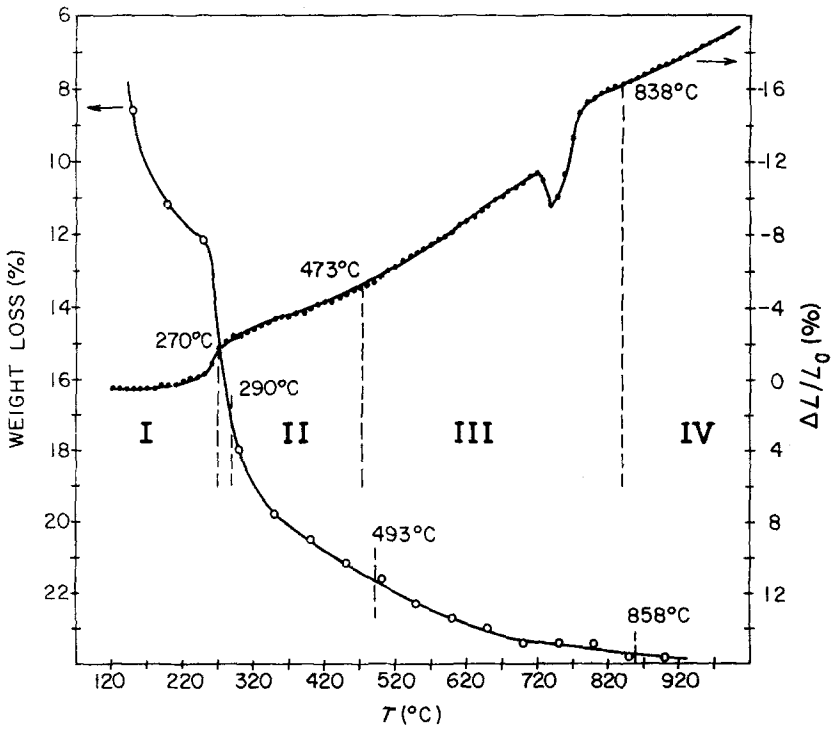


*Figure 11* Linear contraction and weight loss of sample 3.2.

Fig. 14 shows ln $(\Delta L/L_0)$ calculated from Figs 10 to 13 as a function of the inverse of absolute temperature $(1000/T)$. This kind of plot makes it possible to differentiate the steps that take place during densification. The existence of several straight lines indicates, according to the constant-rate-of-heating (CRH) technique [26], that there are as many sintering steps in subsequent temperature ranges. Each step is characterized by a distinctive $Q$ value (apparent activation energy) and $n$ value (exponent of the sintering law), both of which govern the densification process. It has been demonstrated [26] that the CRH technique (a non-isothermal technique) yields the same results as isothermal methods, as far as the study of the sintering process is concerned, even in non-ideal conditions or in order to analyse complex systems such as gels.

Both Sample 3.1 as well as 3.2 (Figs 14a and b), shows four straight lines with different slopes. In Sample 3.1 these four straight lines are much more clearly differentiated than in 3.2, and the temperatures at which the slope changes occur are lower than in 3.1, except for the first line. In Samples 3.3 and 3.4 (Figs 14c and d), however, only two lines are observed. The sites indicating sudden expansions in Figs 10 to 13 were not taken into account for least-squares fit of the straight lines in Fig. 14, and will be interpreted below. The temperatures at which slope changes occur in the straight lines represented in Fig. 14 have been marked in the respective linear contraction curves. In the weight-loss curves the dashed lines have been drawn, enhanced by 20° C in order to compensate for the effect of the different heating rates.

The changes in slope of the straight lines in Fig. 14 entail that the apparent activation energy $Q$ and/or exponent $n$ of the sintering law are changed during the overall densification process. In other words, the mechanism which becomes operative in each temperature range undergoes changes. Following Woolfrey and Bannister [26], the slope $m$ determining the steps of the straight lines in Fig. 14 is related to both the apparent process activation energy $Q$ and the exponent $n$ of the sintering law, by means of the following equation:

$$m = \frac{-Q}{1000R\,(n+1)} \tag{3}$$

Considering that for an activated process the slope of the straight lines, $\ln(\Delta L/L_0) = f(1000/T)$, is $-E_a/1000R$ (Equation 2), the activation energy can be expressed as

$$E_a = Q/(n+1) \tag{4}$$

In Table IV the activation energy values are shown as calculated from the slopes of the straight lines represented in Fig. 14, with $R = 8.31\,\mathrm{J\,mol^{-1}\,K^{-1}}$. The activation energy values are proportional to $Q/(n+1)$, which in turn defines the mechanism which becomes operative in each densification stage.

Segments I in Fig. 14 show the greatest activation energy. The trend observed when increasing the $B_2O_3$ content points towards a decrease in activation energy, which fact suggest that the presence of $B_2O_3$ could favour the first mechanism which operates during densification. As this first segment reaches at most 290° C, most probably a capillary contraction mechanism is involved, due to the loss of organic groups

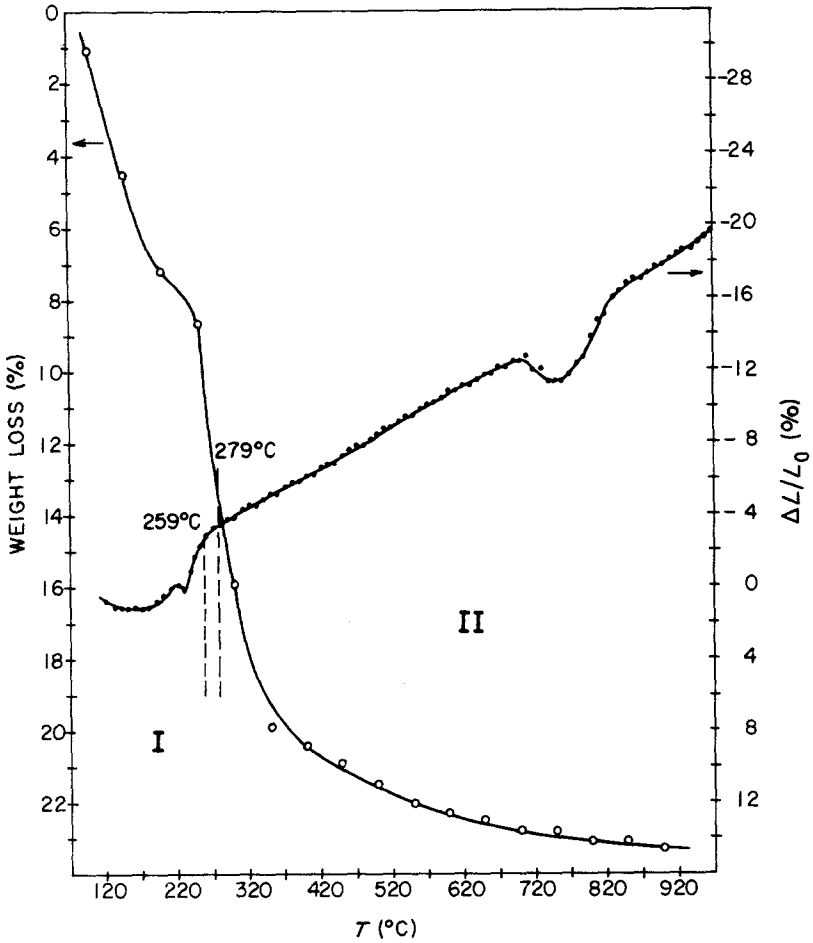


*Figure 12* Linear contraction and weight loss of sample 3.3.

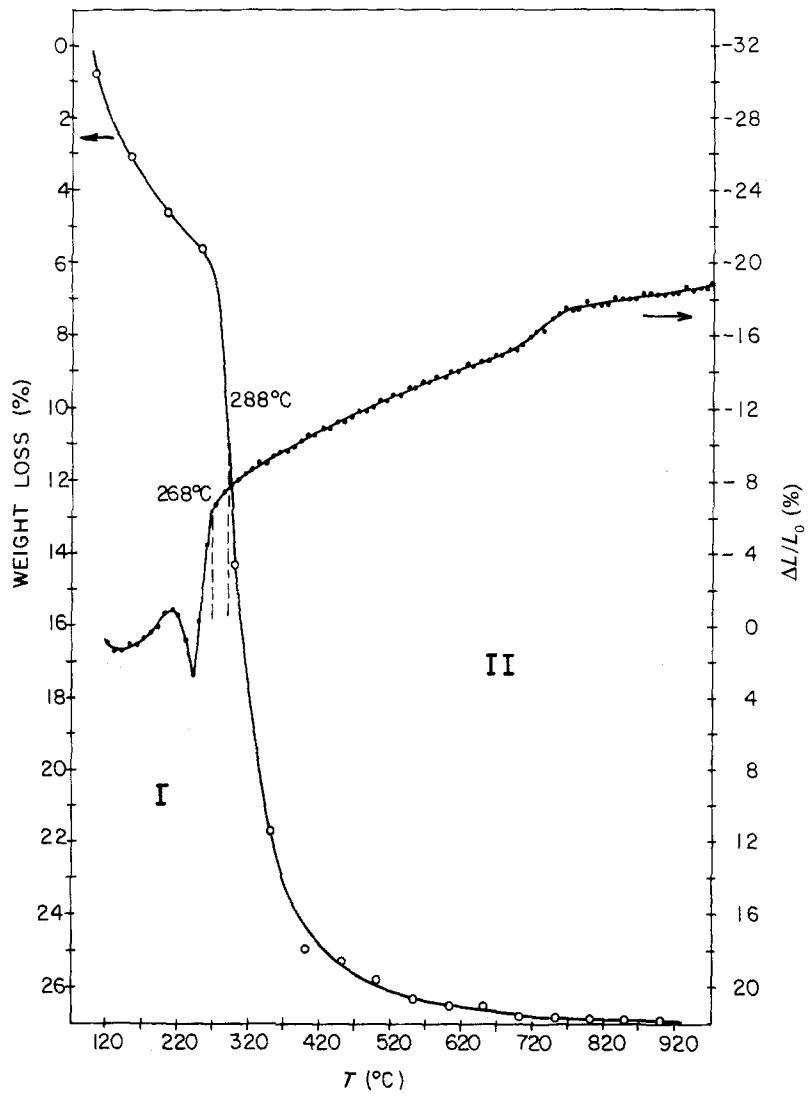


*Figure 13* Linear contraction and weight loss of sample 3.4.

and water. The DTA data obtained confirm this hypothesis.

Segments II in Fig. 14 show rather low activation energy values and different temperature ranges for each of the four samples. For Samples 3.1 and 3.2 this segment ends near 475° C, whereas for the other two samples it extends up to 900° C. The fact that for the two samples with a greater $B_2O_3$ content (3.1 and 3.2) a third segment appears, can be explained in terms of a third mechanism becoming operative at higher temperatures, which either does not exist or is not detectable in the gels with a relatively higher $SiO_2$ content (3.3 and 3.4). Actually, Segment II could be due to a condensation–polymerization mechanism with loss of ≡Si–OH groups. In Fig. 15 gel densities are plotted against temperature. The gels are shown to densify very gradually up to 300 or 400° C, after which the density increases much more rapidly. This can be attributable to ≡Si–OH and =B–OH condensation. If the particles in the gel are rich in $SiO_2$, the effect derived from silanol condensation is predominant and gives rise to ≡Si–O–Si≡ bonds (Samples 3.3 and 3.4), thus masking the =B–OH group condensation with the silanols.

If however, the $B_2O_3$ content is above 30 mol % (Samples 3.1 and 3.2), this latter effect, which originates ≡Si–O–B= bonds, becomes visible (Segments III), irrespective of the fact that Segments II show silanol condensation. Thus in the samples containing 30 and 40 mol % $B_2O_3$ (3.1 and 3.2) a differentiation can be made between contractions due to ≡Si–OH condensation and those due to =B–OH condensation.

The activation energies are greater in Segments III than in Segments II. This fact can be explained through the greater affinity of hydroxyls to boron than to silicon, as $B_2O_3$ is more acid than $SiO_2$ [9]. Hence water release from =B–OH groups is less favoured.

In Samples 3.1 and 3.2 (Figs 14a and b) a further densification mechanism takes place at higher temperatures (Segments IV) characterized by low activation energies (Table IV). In the sample containing 30 mol % $B_2O_3$ (3.2) this segment is very short, as it only sets in above 840° C. In the 40 mol % $B_2O_3$ sample (3.1) Segment IV begins near 653° C, probably due to the higher $B_2O_3$ content which could favour the

TABLE IV Activation energy values calculated from Fig. 14

| Sample No. | $E_a$ (kJ mol$^{-1}$ K$^{-1}$) | | | |
|---|---|---|---|---|
| | Segment I | Segment II | Segment III | Segment IV |
| 3.1 | 125.81 | 9.64 | 40.74 | 11.69 |
| 3.2 | 256.97 | 15.81 | 21.22 | 12.33 |
| 3.3 | 236.34 | 13.90 | – | – |
| 3.4 | 406.63 | 7.79 | – | – |

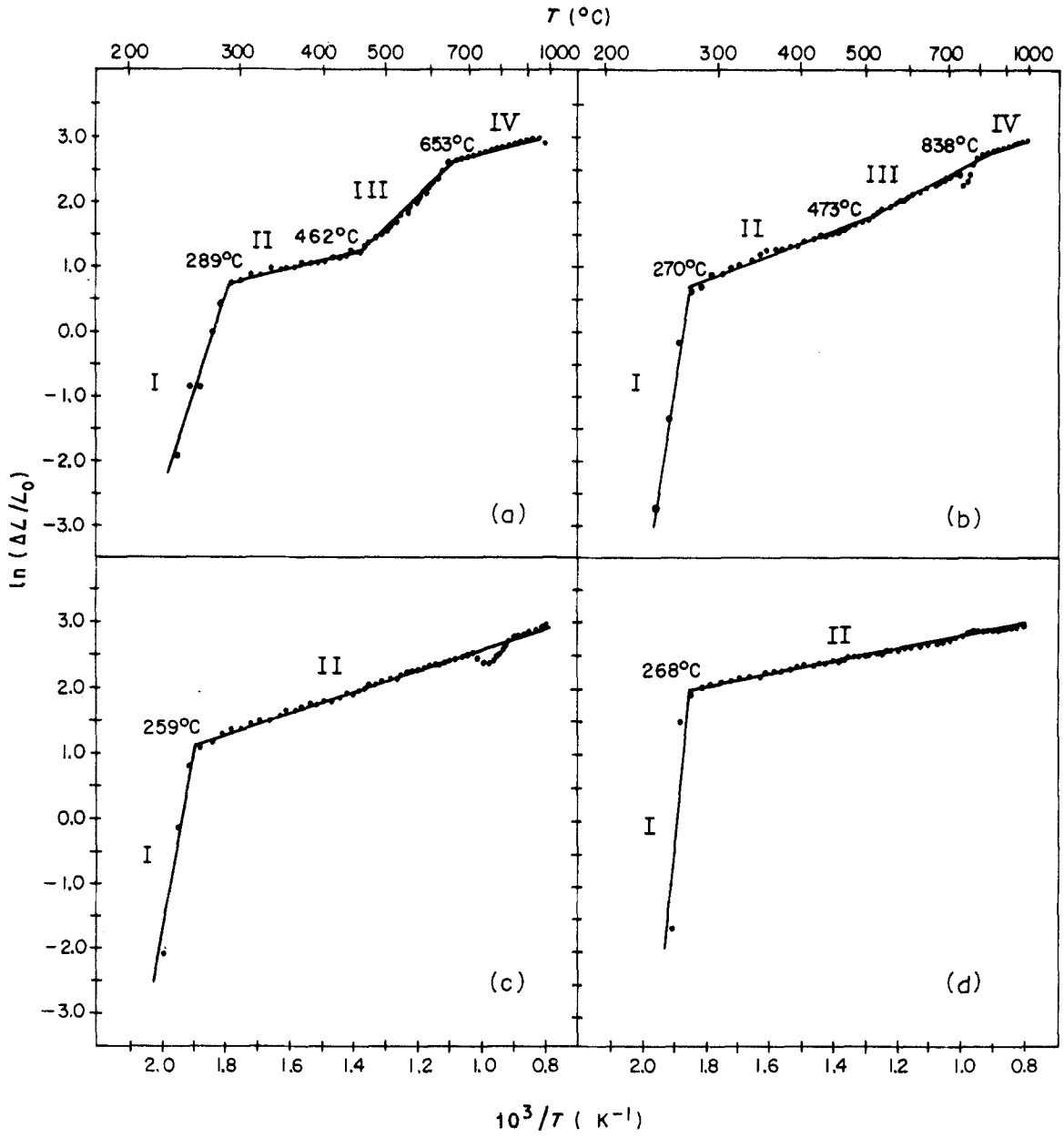


*Figure 14* Logarithmic representation of linear contraction against the inverse of the absolute temperature: (a) 3.1, (b) 3.2, (c) 3.3, (d) 3.4.

sintering process by a viscous flow mechanism. For the samples with a $B_2O_3$ content below 30 mol % the viscous flow-like mechanism is assumed to occur at higher temperatures than those tested (up to 990° C).

In Sample 3.1 (Figs 10 and 14a), from 940° C an expansion phenomenon can be observed which is attributed to gel swelling. Other authors have observed and studied this phenomenon in gels heat-treated above the densification temperature [12, 27, 28]. The small and local expansions shown in Figs 11 to 13 could be indicative of a network reordering process due to the existence of a particle-size distribution as a consequence of compositional complexity of the samples.

## 4. Conclusions

The materials prepared in this paper show a particular evolution with temperature due to the method used for synthesis. The thermal behaviour of the gels is determined by the relatively small amounts of water that were used in the hydrolysis of the alkoxides. The data obtained from DTA–TGA and NIR spectroscopy explain the following situations:

(a) incomplete hydrolysis in the sol of the precursors;

(b) the existence of residual organic groups up to 300° C, until they undergo combustion; and

(c) the existence of a great number of $OH^-$ groups of different natures, which at low temperatures ( < 300° C) may undergo positional changes on the gel particle surface.

With regard to the structure of the gel, the fact is especially relevant that these materials do not devitrify or crystallize in the experimental heat-treatment temperature range up to 800° C. The presence of $B_2O_3$ and the absence of alkalis determine suitable conditions to inhibit silica crystallization. In addition, IR spectroscopy brought to light the existence of absorption bands due to a silica network, as well as to mixed Si–O–B bonds. These latter are situated in the more external positions of the silica particles, as confirmed by the frequency and the relative intensity presented by this vibration band. The absence of B–O–B vibration bands indicates that the whole of the boron

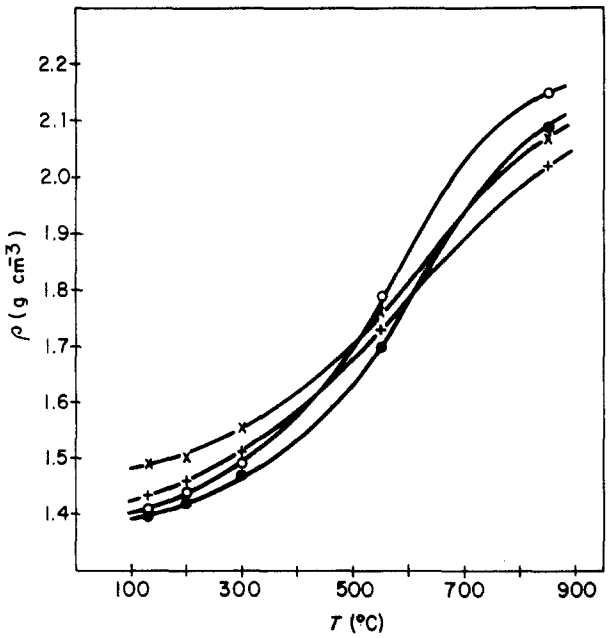


*Figure 15* Thermal evolution of the gel densities: (●) 3.1, (x) 3.2, (+) 3.3, (○) 3.4.

content in the samples is incorporated to build up mixed Si–O–B links. It has been demonstrated that at low temperature the B–O bonds are essentially non-bridge links, which at latter stages evolve towards terminal Si–O–B bonds.

The incorporation of $B_2O_3$ in a silica gel diminishes the process activation energy and favours sintering. Gel densification relies on several mechanisms. At low $B_2O_3$ concentrations two mechanisms become active: capillary contraction due to the loss of water and organic groups, and condensation–polymerization contraction with water release from ≡Si–OH groups. On increasing the $B_2O_3$ content the two mechanisms continue to be operative, with the differentiation between ≡Si–OH and =B–OH group condensation. In addition, from 40 mol % $B_2O_3$ viscous flow-like sintering occurs at higher temperatures.

## References


1. H. DISLICH, *J. Non-Cryst. Solids* **73** (1985) 599.
2. E. M. RABINOVICH, D. W. JOHNSON Jr, J. B. MACCHESNEY and E. M. VOGEL, *J. Amer. Ceram. Soc.* **66** (1983) 688.
3. J. PHALIPPOU, M. PRASSAS and J. ZARZYCKI, *J. Non-Cryst. Solids* **48** (1982) 17.
4. R. JABRA, J. PHALIPPOU and J. ZARZYCKI, *Rev. Chim. Min.* **16** (1979) 245.
5. L. BEYS, M. ABENOZA, P. HILLAIRE and J. PHALIPPOU, *J. Phys. Colloque C9.* Sup. No. 12, **43** (1982) C9-355.
6. M. NOGAMI and Y. MORIYA, *J. Non-Cryst. Solids.* **48** (1982) 359.
7. D. M. HAALAND and C. J. BRINKER, *Mat. Res. Soc. Symp. Proc.* **32** (1984) 267.
8. T. WOIGNIER, J. PHALIPPOU and J. ZARZYCKI, *J. Non-Cryst. Solids* **63** (1984) 117.
9. M. NOGAMI, *Commun. J. Amer. Ceram. Soc.* **67** (1984) C-258.
10. M. DECOTTIGNIES, J. PHALIPPOU and J. ZARZYCKI, *J. Mater. Sci.* **13** (1978) 2605.
11. M. PRASSAS and L. L. HENCH, in "Ultrastructure Processing of Ceramics, Glasses and Composites", edited by L. L. Hench and D. R. Ulrich (Wiley, New York, 1984) p. 100.
12. M. PRASSAS, J. PHALIPPOU and L. L. HENCH, *J. Non-Cryst. Solids* **63** (1984) 375.
13. M. A. VILLEGAS and J. M. FERNANDEZ NAVARRO, in Proceedings of 1st International Workshop on Non-Crystalline Solids, San Feliú, May 1986, edited by M. D. Baró and N. Clavaguera (World Scientific, Philadelphia, 1986) p. 433.
14. *Idem., J. Mater. Sci.* **23** (1988) 2142–52.
15. A. S. TENNEY and J. WONG, *J. Chem. Phys.* **56** (1972) 5516.
16. A. BERTOLUZZA, C. FAGNANO, M. A. MORELLI, V. GOTTARDI and M. GUGLIELMI, *J. Non-Cryst. Solids* **48** (1982) 117.
17. D. M. DODD and D. B. FRASER, *J. Appl. Phys.* **37** (1966) 3911.
18. C. K. WU, *J. Amer. Ceram. Soc.* **63** (1980) 453.
19. R. F. BARTHOLOMEW, B. L. BUTTLER, H. L. HOOVER and C. K. WU, *ibid.* **63** (1980) 481.
20. R. F. BARTHOLOMEW, *J. Non-Cryst. Solids* **56** (1983) 331.
21. J. ACOCELLA, M. TOMOZAWA and E. B. WATSON, *ibid.* **65** (1984) 355.
22. D. L. WOOD, E. M. RABINOVICH, D. W. JOHNSON Jr, J. B. MACCHESNEY and E. M. VOGEL, *J. Amer. Ceram. Soc.* **66** (1983) 693.
23. F. ORGAZ and H. RAWSON, *J. Non-Cryst. Solids* **82** (1986) 57.
24. H. SCHMIDT, A. KAISER, H. PLAZET and H. SCHOLZE, *J. Phys. Colloque C9,* Sup. No. 12, **43** (1982) C9-278.
25. M. A. VILLEGAS and J. M. FERNANDEZ NAVARRO, *Bol. Soc. Esp. Ceram. Vidr.* **26** (1987) 235.
26. J. L. WOOLFREY and M. J. BANNISTER, *J. Amer. Ceram. Soc.* **55** (1972) 390.
27. J. PHALIPPOU, T. WOIGNIER and J. ZARZYCKI, in "Ultrastructure Processing of Ceramics, Glasses and Composites", edited by L. L. Hench and D. R. Ulrich (Wiley, New York, 1984) p. 70.
28. F. ORGAZ and M. P. CORRAL, in Proceedings of 1st International Workshop on Non-Crystalline Solids, San Feliú, May 1986, edited by M. D. Baró and N. Clavaguera (World Scientific, Philadelphia, 1986) p. 423.


*Received 26 June*
*and accepted 22 September 1987*